

Magnetization curves of deposited finite spin chains

Henning-Timm Langwald* and Jürgen Schnack†

Fakultät für Physik, Universität Bielefeld, Postfach 100131, D-33501 Bielefeld, Germany

(Dated: December 4, 2013)

The characterization and manipulation of deposited magnetic clusters or molecules on surfaces is a prerequisite for future utilization. For this purpose spin-flip inelastic electron tunneling spectroscopy using a scanning tunneling microscope proved to be very precise in determining e.g. exchange constants in deposited finite spin chains in the meV range. In this Letter we provide numerical justification for the underlying assumptions made in such investigations. To this end we study the impurity magnetization of antiferromagnetic chains for varying couplings to a conduction electron band of a metal substrate. We show under which circumstances the screening of a part of the system enables one to deduce molecular parameters of the remainder from level crossings in an applied field.

PACS numbers: 73.20.Hb, 75.30.Cr, 75.30.Gw, 75.50.Xx

Keywords: NRG, Magnetization, Deposited Magnetic Molecules

Introduction—The question whether and how deposited magnetic clusters or molecules change their magnetic properties when deposited on a metallic substrate is of fundamental importance especially in view of possible applications as next generation storage devices or magnetic logic circuits [1–7]. One experimental method to investigate local magnetic properties is spin-flip inelastic electron tunneling spectroscopy with a scanning tunneling microscope [1, 8]. In this method jumps of the differential conductivity signal transitions between magnetic levels of the deposited entity, of course under the assumption of a weak coupling to the substrate. Following this philosophy the authors of Ref. [8] conjectured the strength of superexchange interactions in deposited molecular nanomagnets. The latter were constructed by depositing layers of cobalt phthalocyanine molecules which self-organized in a stacked manner so that the cobalt ions formed finite spin chains on the substrate. This arrangement is sketched in Fig. 1 (a).

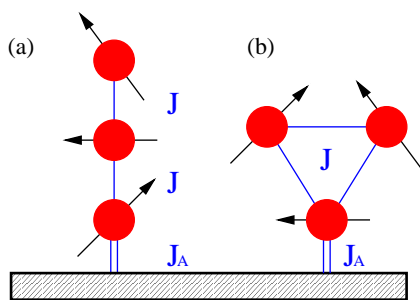


FIG. 1: (Color online) Sketch of the trimer configuration (a) investigated in Ref. [8]: stacked magnetic centers interact via an exchange coupling J , the lowest moment is coupled to the metal surface with strength J_A . J and J_A are unknown, J shall be derived from experimental data. (b) shows a triangular configuration discussed later in this Letter.

When interpreting the observed structure of magnetic levels in such measurements one has to conjecture whether and how much of the deposited magnetic mo-

ment is screened by the conduction electrons, since this has a great influence on the magnetic properties of the remainder. In Ref. [8] it was deduced that the Co^{2+} spin with $s = 1/2$ closest to the surface was completely Kondo-screened and therefore the observed magnetic levels should result from a practically uncoupled remainder of $(N - 1)$ spins.

In this Letter we investigate by means of the Numerical Renormalization Group method (NRG) [9–11] numerically exactly how the magnetic properties of deposited structures as those shown in Fig. 1 depend on the exchange coupling J_A to the substrate’s conduction electrons, the internal exchange coupling J , and the applied magnetic field B at low temperature T . Depending on J_A the screening can vary between full screening and partial screening of the spin-1/2 closest to the surface. In the case of full screening the magnetic properties of the deposited entity are indeed identical to those of the remaining spin system without the screened spin.

For our investigations we employ a single-channel single-impurity Kondo model as a minimal model to describe the correlations induced by the exchange interaction between the conduction electrons of the non-magnetic metal and one spin of the magnetic molecule [12, 13]. As already demonstrated in Ref. [14] the magnetization steps due to ground state level crossings in an applied magnetic field can be used as fingerprints of the underlying spin model. This will be shown by investigating different sizes of chains as well as triangular arrangements of magnetic moments.

Reminder on NRG—In order to model a molecule and its coupling to a surface we use the following Hamiltonian which consists of three parts [12–14]:

$$\tilde{H} = \tilde{H}_{\text{electrons}} + \tilde{H}_{\text{coupling}} + \tilde{H}_{\text{impurity}}, \quad (1)$$

$$\tilde{H}_{\text{electrons}} = \sum_{i \neq j, \sigma} t_{ij} d_{i\sigma}^\dagger d_{j\sigma} + g\mu_B B \sum_i \xi_i^z. \quad (2)$$

The first part $\tilde{H}_{\text{electrons}}$ represents non-interacting electrons on a lattice. The hopping parameter t_{ij} is non-zero

only if the lattice sites i, j are nearest neighbours. $d_{i\sigma}^\dagger$ and $d_{j\sigma}$ are fermionic creation and annihilation operators for electrons with spin direction σ . The interaction with an external magnetic field B is given by the Zeeman term with s_i^z representing the effective electron spin at lattice site i , g the g -factor and μ_B the Bohr magneton. The second part $\tilde{H}_{\text{impurity}}$ models the impurity, i.e., the molecule or chain via an effective Heisenberg model for all connected spins \tilde{S}_i and a Zeeman term. J_{ij} is the interaction between spins i and j and antiferromagnetic for $J_{ij} > 0$,

$$\tilde{H}_{\text{impurity}} = 2 \sum_{i < j} J_{ij} \tilde{S}_i \cdot \tilde{S}_j + g \mu_B B \sum_i \tilde{S}_i^z. \quad (3)$$

The last part $\tilde{H}_{\text{coupling}}$ describes the Kondo-like interaction of the molecule with the surface. The coupling constant J_A is positive for antiferromagnetic coupling

$$\tilde{H}_{\text{coupling}} = 2 \cdot J_A \cdot \tilde{S}_1 \cdot \tilde{S}_0. \quad (4)$$

To calculate thermodynamic values within this model we use Wilson's Numerical Renormalization Group (NRG) with the discretization scheme proposed by Žitko and Pruschke [15, 16] and a z -averaging for 2 values. A constant density of states is assumed.

It is possible that in reality molecular orbitals of phthalocyanine molecules hybridize with surface states, compare e.g. [7, 17–21]. Our approach, like others [12, 13], simplifies the situation to a point where the deposited molecule is reduced to its spin degrees of freedom which interact with the metal's conduction electrons.

Results and interpretation—Before we discuss our numerical results of a finite spin chain interacting with a metal substrate we would like to shortly look at a free three-site chain of spins $s = 1/2$. Its levels split under the influence of an applied magnetic field as depicted on the l.h.s. of Fig. 2. At a certain magnetic field value $B_c = 3 \cdot J/(g\mu_B)$ the lowest ($S = 1/2, M = -1/2$) and ($S = 3/2, M = -3/2$) levels cross. If the lowest spin of the trimer would be completely screened, the remaining dimer would possess a different level scheme with a different crossing field $B_c = 2 \cdot J/(g\mu_B)$ as depicted on the r.h.s. of Fig. 2. Therefore, inferring J from spectroscopic data or equivalently from crossing fields strongly depends on the degree of screening.

In the following we discuss the so-called impurity magnetization, i.e. the thermal expectation value of molecular magnetic moment $\sum_i \tilde{S}_i^z$ as a function of the applied field for various couplings to the substrate. In order to work with reasonable numbers we set the intramolecular coupling to $J = 1$ meV and the half-bandwidth of the metal to $W = 1$ eV. As the temperature we choose $T \approx 2 \cdot 10^{-4} W/k_B \approx 2.36$ K, which is lower than the intramolecular coupling, but not too low so that thermodynamic functions are still smooth [23].

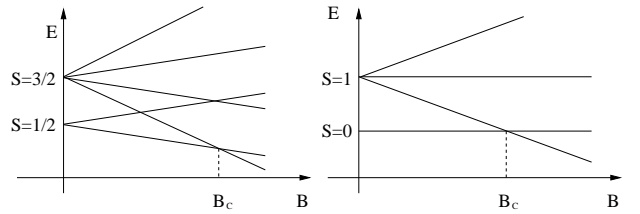


FIG. 2: (Color online) Sketch of the Zeeman levels of a trimer of three spins $s = 1/2$ (l.h.s.) and of a dimer of two spins $s = 1/2$ (r.h.s.).

After looking at the lowest Zeeman levels of a free trimer we now consider the coupling of such a trimer to a surface as described by Eq. (4) and shown in Fig. 1 (a). The strength of the coupling is parametrized by J_A . The impurity magnetization curves depicted in Fig. 3 cover the whole range from the free ($J_A = 0$) or weakly coupled case to the strongly coupled case, which is reached for $J_A \gtrsim 0.5$ eV. While the case $J_A = 0$ coincides with the discussed free trimer by construction, the strongly coupled case coincides with the magnetization curve of a free dimer.

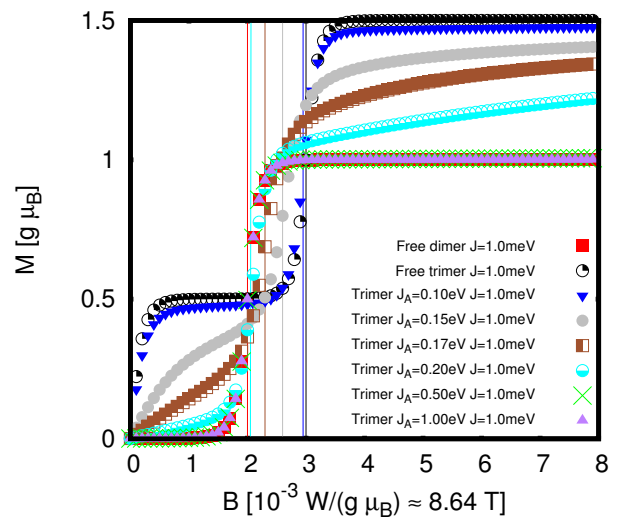


FIG. 3: (Color online) Impurity magnetization vs. magnetic field for the trimer shown in Fig. 1 (a); vertical lines mark the crossing fields for various scenarios; $T \approx 2 \cdot 10^{-4} W/k_B \approx 2.36$ K.

Additionally to the magnetization curves, Fig. 3 includes the crossing fields for various scenarios which can be derived from the magnetization curves. The vertical lines marking these fields shift from the analytical solution of a free trimer towards the analytical solution of a free dimer for increasing coupling to the substrate. The analytical solutions thus are boundaries for the crossing field independent of the coupling J_A .

Focusing on the strong coupling regime, Fig. 4 shows

variations of the couplings J and J_A . Within this regime, i.e. for strong enough J_A , the magnetization curves are independent of J_A and coincide with the solution for a free dimer and thus depend on the coupling J in the same way the analytical solution does. In particular the crossing field is given by $B_c = 2 \cdot J / (g\mu_B)$. Given a strong enough coupling to reach the strong coupling regime it is therefore possible to derive J from the crossing field. Our investigation also shows that the maximum uncertainty in the determination of J , in the case of unknown J_A , is given by the difference between the (analytical) solutions for the crossing field of the unscreened system and the fully screened one.

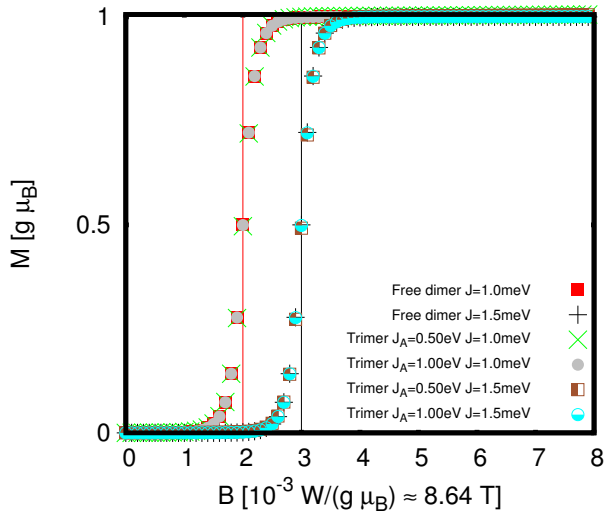


FIG. 4: (Color online) Impurity magnetization vs. magnetic field for the strong coupling case; vertical lines mark crossing fields; $T \approx 2 \cdot 10^{-4} W/k_B \approx 2.36$ K. The magnetization curve depends only on J , not on J_A in the strong coupling case.

Similar results are obtained if a triangular structure is used, where all three spins couple to each other, but still only one couples to the substrate, compare Fig. 1 (b). For the case of $J_A = 0$ analytical results can be obtained for both trimer chain and triangle [22]. These show that the magnetization curves and thus the crossing fields coincide for $T \rightarrow 0$. Figure 5 shows the magnetization curves of triangle and trimer chain for finite temperature where the curves for $J_A = 0$ feature small differences. For intermediate couplings to the substrate, $0 < J_A < 0.5$ eV, the differences are more pronounced.

Figure 5 furthermore shows the case of strong coupling to the substrate, again $J_A \gtrsim 0.5$ eV. In this case trimer chain and triangle are indistinguishable on the basis of their magnetization curves and thus their crossing fields, compare \times -symbols and upright triangles in Fig. 5.

After considering the triangle, and thus a slightly different structure of the impurity, we now come back to chain-like impurities and extend our original trimer chain

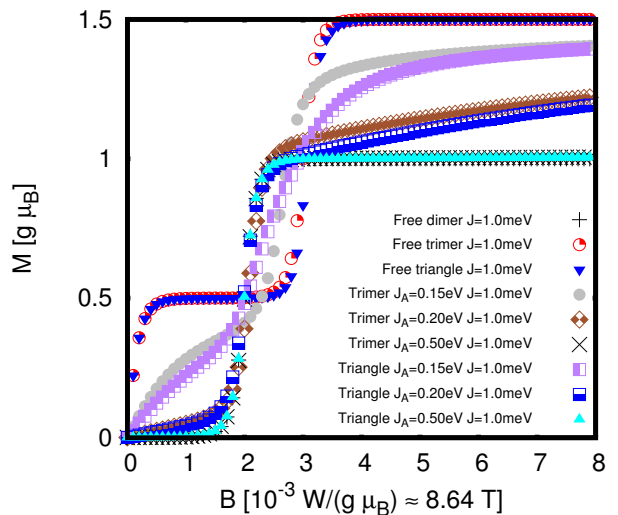


FIG. 5: (Color online) Impurity magnetization vs. magnetic field for trimeric and triangular impurities; $T \approx 2 \cdot 10^{-4} W/k_B \approx 2.36$ K.

to four and five spins analogous to the experiment in Ref. [8]. Figure 6 shows the magnetization curves of a tetramer chain for various couplings to the substrate.

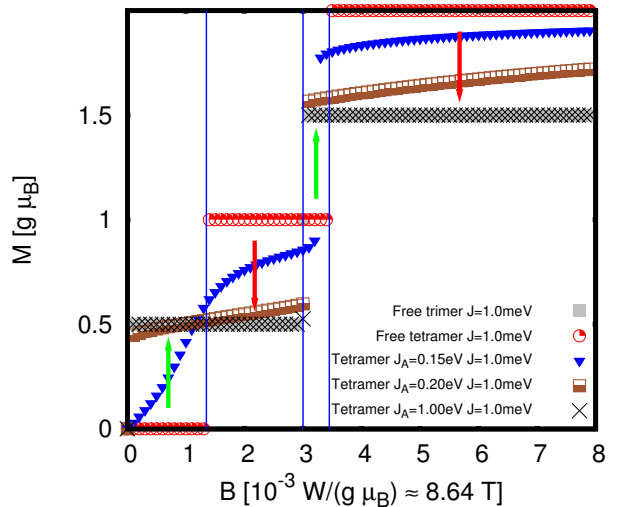


FIG. 6: (Color online) Impurity magnetization vs. magnetic field for tetramer impurities; vertical lines separate areas with an increase (green arrows) or decrease (red arrows) in magnetization by strongly coupling the free system to the substrate; $T \approx 6 \cdot 10^{-8} W/k_B \approx 6.92 \cdot 10^{-4}$ K.

The curves are affected by the coupling to the substrate in a similar way to those of the trimer chain with the crossing fields decreasing for stronger couplings. In the strong coupling regime the tetramer chain then shows the same magnetization curve and crossing field as the free

trimer. Analogously the magnetization curve and crossing fields of the pentamer chain, as depicted in Fig. 7, coincide with those of the free tetramer in the strong coupling limit.

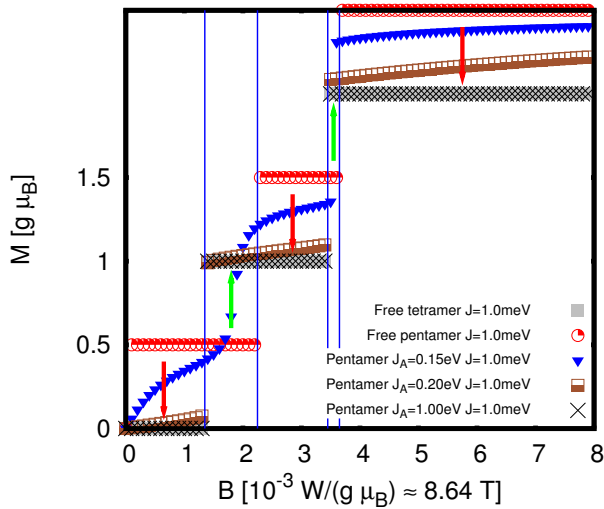


FIG. 7: (Color online) Impurity magnetization vs. magnetic field for pentamer impurities; vertical lines separate areas with an increase (green arrows) or decrease (red arrows) in magnetization by strongly coupling the free system to the substrate; $T \approx 6 \cdot 10^{-8} W/k_B \approx 6.92 \cdot 10^{-4} K$.

Unlike the other figures, Figures 6 and 7 include vertical lines which confine areas of (practically) constant magnetization for the free and the strongly coupled chains at a now very low temperature of $T \approx 6 \cdot 10^{-8} W/k_B \approx 6.92 \cdot 10^{-4} K$. For those areas an arrow indicates whether the magnetization is increased (green arrow) or decreased (red arrow) due to the coupling to the substrate. For the tetramer chain with its ground state spin of $S = 0$ the screening leads to an increased magnetization at (and thus a response to) small magnetic fields. In contrast the magnetization for the pentamer chain with its ground state spin of $S = 1/2$ is decreased at small magnetic fields and thus will not respond to small magnetic fields in the strong coupling regime.

Summarizing, NRG calculations of the impurity magnetization provide a very valuable tool in order to rationalize experimental assumptions and results as for instance those of Ref. [8]. Future investigations of more complicated impurities as for instance magnetic molecules with non-Heisenberg terms in the Hamiltonian pose no problem, but NRG is technically limited to single-channel (or with massive super computing time to two-channel) contacts. This is due to the rapidly growing Hilbert space dimension which is already for two channels the square of the dimension for one channel.

Acknowledgment

This work was supported by the Deutsche Forschungsgemeinschaft through Research Unit 945. Computing time at the Leibniz Computing Center in Garching is gratefully acknowledged. We thank Martin Höck for fruitful discussions.

* Electronic address: langwald@physik.uni-bielefeld.de

† Electronic address: jschnack@uni-bielefeld.de

- [1] C. F. Hirjibehedin, C. P. Lutz, and A. J. Heinrich, *Science* **312**, 1021 (2006).
- [2] C. F. Hirjibehedin, C.-Y. Lin, A. F. Otte, M. Ternes, C. P. Lutz, B. A. Jones, and A. J. Heinrich, *Science* **317**, 1199 (2007).
- [3] H. Wende, M. Bernien, J. Luo, C. Sorg, N. Ponpandian, J. Kurde, J. Miguel, M. Piantek, X. Xu, P. Eckhold, et al., *Nat. Mater.* **6**, 516 (2007).
- [4] M. Mannini, F. Pineider, P. Saintavrit, C. Danieli, E. Otero, C. Sciancalepore, A. M. Talarico, M.-A. Arrio, A. Cornia, D. Gatteschi, et al., *Nat. Mater.* **8**, 194 (2009).
- [5] D. Wegner, R. Yamachika, X. Zhang, Y. Wang, T. Baruah, M. R. Pederson, B. M. Bartlett, J. R. Long, and M. F. Crommie, *Phys. Rev. Lett.* **103**, 087205 (2009).
- [6] M. Bernien, J. Miguel, C. Weis, M. E. Ali, J. Kurde, B. Krumme, P. M. Panchmatia, B. Sanyal, M. Piantek, P. Srivastava, et al., *Phys. Rev. Lett.* **102**, 047202 (2009).
- [7] J. Brede, N. Atodiresei, S. Kuck, P. Lazić, V. Caciuc, Y. Morikawa, G. Hoffmann, S. Blügel, and R. Wiesendanger, *Phys. Rev. Lett.* **105**, 047204 (2010).
- [8] X. Chen, Y.-S. Fu, S.-H. Ji, T. Zhang, P. Cheng, X.-C. Ma, X.-L. Zou, W.-H. Duan, J.-F. Jia, and Q.-K. Xue, *Phys. Rev. Lett.* **101**, 197208 (2008).
- [9] R. Bulla, T. A. Costi, and T. Pruschke, *Rev. Mod. Phys.* **80**, 395 (2008).
- [10] K. G. Wilson, *Rev. Mod. Phys.* **55**, 583 (1983).
- [11] K. G. Wilson, *Rev. Mod. Phys.* **47**, 773 (1975).
- [12] C. Romeike, M. R. Wegewijs, W. Hofstetter, and H. Schoeller, *Phys. Rev. Lett.* **96**, 196601 (2006).
- [13] C. Romeike, M. R. Wegewijs, W. Hofstetter, and H. Schoeller, *Phys. Rev. Lett.* **97**, 206601 (2006).
- [14] M. Höck and J. Schnack, *Phys. Rev. B* **87**, 184408 (2013).
- [15] R. Žitko and T. Pruschke, *Phys. Rev. B* **79**, 085106 (2009).
- [16] R. Žitko, *Comput. Phys. Commun.* **180**, 1271 (2009), ISSN 0010-4655.
- [17] L. Scudiero, D. E. Barlow, U. Mazur, and K. W. Hipps, *J. Am. Chem. Soc.* **123**, 4073 (2001).
- [18] D. E. Barlow, L. Scudiero, and K. W. Hipps, *Langmuir* **20**, 4413 (2004), pMID: 15969147.
- [19] A. Zhao, Q. Li, L. Chen, H. Xiang, W. Wang, S. Pan, B. Wang, X. Xiao, J. Yang, J. G. Hou, et al., *Science* **309**, 1542 (2005).
- [20] L. Gao, W. Ji, Y. B. Hu, Z. H. Cheng, Z. T. Deng, Q. Liu, N. Jiang, X. Lin, W. Guo, S. X. Du, et al., *Phys. Rev. Lett.* **99**, 106402 (2007).
- [21] S. Stepanow, P. S. Miedema, A. Mugarza, G. Ceballos,

- P. Moras, J. C. Cezar, C. Carbone, F. M. F. de Groot, and P. Gambardella, *Phys. Rev. B* **83**, 220401 (2011).
- [22] D. Mentrup, H.-J. Schmidt, J. Schnack, and M. Luban, *Physica A* **278**, 214 (2000).
- [23] Since the thermodynamic functions have to be evaluated

for every magnetic field value, too abruptly varying functions would need more supporting points. Already now each NRG curve in any of the figures needs a rather long time on a supercomputer.